The Synthesis and Characterization of Potassium 2,2′-Bipyridinetetranitroruthenate

Daniel A. Freedman,*,† Daron E. Janzen, and Kent R. Mann*

Department of Chemistry, State University of New York at New Paltz, New Paltz, New York 12561, and Department of Chemistry, University of Minnesota, Minneapolis, Minnesota 55455

Received May 24, 2001

We report a convenient synthesis of $K_2[Ru(bpy)(NO_2)_4]$ via the *thermal* displacement of benzene from [(Bz)-Ru(bpy)Cl]Cl (Bz = η^6-C_6H_6; bpy = 2,2′-bipyridine) by nitrite ion in methanol solution. $K_2[Ru(bpy)(NO_2)_4]$ has been fully characterized by elemental analysis, X-ray crystallography, and ^{1}H NMR, IR, UV−vis, and emission spectroscopy. Reaction of $K_2[Ru(bpy)(NO_2)_4]$ with pyridine under mild or forcing conditions produces *fac*-K[Ru-(bpy)$(NO_2)_3$(py)] and *cis*-$[Ru(NO_2)_2(bpy)(py)_2]$ (py = pyridine), respectively. We report full characterization data for these compounds, including crystal structures. The dπ(Ru) → π*(bpy) charge-transfer band in the electronic spectra of $K_2[Ru(bpy)(NO_2)_4]$ and *fac*-[Ru(bpy)$(NO_2)_3$(py)] displays a significant solvent dependence. The energy of the absorption band correlates linearly with the Gutmann solvent acceptor number. The solvatochromic response of these nitro complexes is essentially identical to that of the analogous cyanide complexes, indicating that the mechanism previously proposed to explain the solvatochromism of the cyanide complexes may need to be reexamined.

Introduction

We have been interested for some time in the synthetic applications of the photochemical displacement of benzene from M(II) complexes (M = Fe, Ru, Os).[1−4] Most recently, one of our groups has used this strategy to prepare the $[Ru(bpy)(CN)_4]^{2-}$ ion via the photolysis of [(Bz)Ru(bpy)Cl]Cl with cyanide in methanol solution (Reaction 1).[4] This route provided a significant improvement in both yield and ease of preparation of this previously prepared complex.[5]

$$[(Bz)Ru(bpy)Cl]Cl \xrightarrow[MeOH]{h\nu,\ \text{excess KCN}} [Ru(bpy)(CN)_4]^{2-} + \text{benzene} + 2KCl \quad (1)$$

The large solvatochromic shifts in the intense UV−vis absorption and emission bands displayed by the $[Ru(bpy)(CN)_4]^{2-}$ ion[6] suggest it as a potential candidate for the construction of environmental sensing devices. Studies of the crystalline salt $(PPN)_2[Ru(bpy)(CN)_4]$ (PPN^+ = bis(triphenylphosphine)-iminium cation) show it to be an excellent solid-state humidity sensor[4] as well as a sensor of low molecular weight alcohols.[7] The UV−vis absorption and emission bands of this salt undergo large, reversible shifts as the humidity level is varied. This salt is one of a small number of examples of well-characterized, crystalline humidity sensors.[8,9] To further study the mechanism for vapochromic shifts in the absorption and emission spectra of metal complexes, we are examining other $[(bpy)RuX_4]^{2-}$ complexes (where X is a monodentate, anionic ligand). Herein, we describe our investigations of the X = NO_2^- complex.

We chose the NO_2^- ligand for several reasons. Like cyanide, nitrite is high in the spectrochemical series,[10] a desirable quality for a sensor because it increases the likelihood that the complex will exhibit room-temperature emission. Additionally, the ability of nitro ligands to transmit environmental influences, such as solvent interactions via lone pairs, should be similar to a cyanide ligand.

Experimental Section

General Considerations. KNO_2, 2,2′-bipyridine, and 4,7,13,16,21,24-hexaoxa-1,10-diazabicyclo[8.8.8]hexacosane ([2.2.2]-crypt) were purchased from Aldrich. $RuCl_3 \cdot xH_2O$ was purchased from Alfa. All synthetic procedures were carried out under an inert Ar or N_2 atmosphere unless otherwise noted. The synthesis and characterization of $[(arene)Ru(bpy)Cl]^+$ complexes have been previously reported.[11] The [(Bz)Ru(bpy)Cl]Cl used in the following syntheses was prepared via a modification of a previously reported procedure.[12] Elemental analyses were performed by QTI Analytical Laboratories. ^{1}H NMR spectra were recorded on JEOL 300 MHz Eclipse or Varian 500 MHz spectrometers. ^{1}H NMR chemical shifts are relative to $(CH_3)_4Si$. UV−vis spectra were recorded on Cary 17 and Ocean Optics spectrometers. IR spectra were recorded on a Perkin-Elmer 1600 FTIR using a multiple internal reflectance accessory. Emission spectra were recorded at room temperature with a Princeton Instruments ST138 UV−vis/NIR sensitive LN_2 cooled/CCD spectrometer. The Winspec v1.6.1.3 software package was used to acquire the emission spectra. The emission spectra (front face detection from optically dense solutions in acetonitrile or solids)

* To whom correspondence should be addressed.
† State University of New York at New Paltz.

(1) Gill, T. P.; Mann, K. R. *Organometallics* **1982**, *1*, 485.
(2) Mann, K. R.; Blough, A. M.; Schrenk, J. L.; Koefod, R. S.; Freedman, D. A.; Matachek, J. R. *Pure Appl. Chem.* **1995**, *65*, 95.
(3) Graf, D. D.; Mann, K. R. *Inorg. Chem.* **1997**, *36*, 141.
(4) Evju, J. K.; Mann, K. R. *Chem Mater.* **1999**, *11*, 1425.
(5) Bignozzi, C. A.; Chiorboli, C.; Indelli, M. T.; Scandola, M. A.; Varani, G.; Scandola, F. *J. Am. Chem. Soc.* **1986**, *108*, 7872.
(6) Timpson, C. J.; Bignozzi, C. A.; Sullivan, B. P.; Kober, E. M.; Meyer, T. J. *J. Phys. Chem.* **1996**, *100*, 2915.
(7) Buss, C. E.; Anderson, C. E.; Pomije, M. K.; Lutz, C. M.; Britton, D.; Mann, K. R. *J. Am. Chem. Soc.* **1998**, *120*, 7783.
(8) Shih, K. C.; Herber, R. H. *Inorg. Chem.* **1992**, *21*, 5444.
(9) Boltinghouse, F.; Abel, K. *Anal. Chem.* **1989**, *61*, 1863.
(10) Hoggard, P. E. and Clanet, P. P. *Polyhedron* **1987**, *6*, 1621.
(11) (a) Robertson, D. R.; Robertson, I. W.; Stephenson, T. A. *J. Organomet. Chem.* **1980**, 202, 309. (b) Kaim, W.; Reinhardt, R.; Sieger, M. *Inorg. Chem.* **1994**, 33, 4453. (c) Dadci, L.; Elias, H.; Frey, U.; Hornig, A.; Koelle, U.; Merbach, A. E.; Paulus, H.; Schneider, J. S. *Inorg. Chem.* **1995**, *34*, 306. (d) Ashby, M. T.; Alguindigue, S. S.; Khan, M. A. *Organometallics* **2000**, *19*, 547.
(12) Freedman, D. A.; Evju, J. K.; Pomije, M. K.; Mann, K. R. *Inorg. Chem.*, in press.

10.1021/ic010548m CCC: $20.00
Published on Web 10/05/2001

were collected from samples irradiated at 435.8 nm with the interference-filtered output of a medium pressure 175 W Hg/Na lamp. The emission spectra were corrected for grating efficiency and detector response.[13]

The UV−vis spectra of $K_2[Ru(bpy)(NO_2)_4]$ and *fac*-$K[Ru(bpy)(NO_2)_3(py)]$ in different solvents were acquired with an Ocean Optics CCD array spectrometer. Solvents were of ACS reagent grade and were used without further purification. The solvent and a small amount of [2.2.2]crypt were added to the cuvette. The ruthenium complex was then added, the solution was stirred, and the spectrum was acquired immediately.

Preparation of $K_2[Ru(bpy)(NO_2)_4]$. A solution of [(Bz)Ru(bpy)Cl]Cl (1.00 g, 2.46 mmol) and KNO_2 (2.09 g, 24.6 mmol) in 50 mL of methanol was purged with nitrogen for 15 min and then refluxed for 4 h. Almost immediately, a bright orange precipitate began to form. The solution was cooled, and the product was filtered off. The product was dissolved in a minimal amount of cold water, filtered through a short column of diatomaceous earth, and precipitated by the addition of methanol and cooling in an ice bath. Filtration and drying in vacuo yielded 0.940 g (73.6% yield) of a bright orange powder. Anal. Calcd for $RuK_2C_{10}H_8N_6O_8$: C, 23.12; H, 1.55; N, 16.18. Found: C, 22.87; H, 1.58; N, 15.74. ^{1}H NMR (500 MHz, D_2O vs DSS) δ: 7.59 ($H^{5,5'}$, unresolved d of d, 2H, $J = 6.5$ Hz); 8.05 ($H^{4,4'}$, unresolved d of d, 2H, $J = 8.0$ Hz); 8.33 ($H^{3,3'}$, d, 2H, $J = 8.5$ Hz); 9.04 ($H^{6,6'}$, d, 2H, $J = 6.0$ Hz). IR (ATR, cm^{-1}): $\nu_{as} = 1342, 1324$; $\nu_{sym} = 1284, 1274$; $\delta_{ONO} = 833, 824, 821, 802$. UV−vis ($H_2O$, nm): 390, 340, 319, 288.

Preparation of *fac*-$K[Ru(bpy)(NO_2)_3(py)]$. A solution of $K_2[Ru(bpy)(NO_2)_4]$ (0.250 g) in water (10 mL) and pyridine (1.0 mL) was stirred for 48 h. The color of the solution slowly changed from orange to reddish-orange. The product was precipitated by adding 20 mL of acetone to the solution and cooling at −15 °C for 2 days. The product was filtered and washed with acetone to give a mixture of reddish-orange powder and needles (0.136 g, 55%). Anal. Calcd for $RuKC_{15}H_{13}N_6O_6\cdot H_2O$: C, 33.90; H, 2.84; N, 15.81. Found: C, 34.21; H, 2.46; N, 15.88. ^{1}H NMR (500 MHz, D_2O vs DSS) δ: 7.09 (H^3 py, unresolved d of d, 2H, $J = 6.5$ Hz); 7.66 ($H^{5,5'}$ bpy and H^4 py, m, 3H); 8.02 ($H^{4,4'}$ bpy, unresolved d of d, 2H, $J = 8.0$ Hz); 8.10 (H^2 py, d, 2H, $J = 5.5$ Hz); 8.23 ($H^{3,3'}$ bpy, d, 2H, $J = 8.5$ Hz); 9.22 ($H^{6,6'}$ bpy, d, 2H, $J = 5.5$ Hz). IR (ATR, cm^{-1}): $\nu_{as} = 1322, 1303$; $\nu_{sym} = 1278, 1212$; $\delta_{ONO} = 822$. UV−vis (H_2O, nm (ϵ/(M^{-1} cm^{-1}))): 419 (2.6×10^3), 345 (5.8×10^3), 313 (1.1×10^4), 285 (1.8×10^4).

Preparation of *cis*-$Ru(NO_2)_2(bpy)(py)_2$. $Ru(NO_2)_2(bpy)(py)_2$ has been prepared previously by a different method.[14] A solution of $K_2[Ru(bpy)(NO_2)_4]$ (0.153 g) in pyridine (10 mL) was purged with nitrogen and refluxed for 14 h. Reliable synthesis required an adjustment of the amount of water in the solution. If the solution was still orange in color, water was added dropwise through the condenser to the refluxing solution until any precipitate dissolved; if the solution was dark red with a dark precipitate present, no water was added. The reflux was continued for another 24 h, and then the solution was cooled to room temperature. The product was collected by filtration and washed with water, acetone, and diethyl ether. The product was isolated as a dark red powder (0.0725 g, 48.3%). Anal. Calcd for $RuC_{20}H_{18}N_6O_4\cdot 0.5\ H_2O$: C, 46.51; H, 3.71; N, 16.27. Found: C, 47.01; H, 3.55; N, 15.57. ^{1}H NMR (500 MHz, DMSO-d_6), δ: 7.13 (H^3 py, unresolved d of d, 4H, $J = 7.5$ Hz); 7.64 (H^4 py, dd, 2H, $J = 8.0, 8.0$ Hz); 7.78 ($H^{5,5'}$ bpy, unresolved d of d, 2H, $J = 6.0$ Hz); 8.02 ($H^{4,4'}$ bpy, unresolved d of d, 2H, $J = 8.0$ Hz); 8.38 (H^2 py, d, 4H, $J = 4.5$ Hz); 8.45 ($H^{3,3'}$ bpy, d, 2H, $J = 8.0$ Hz); 9.57 ($H^{6,6'}$ bpy, d, 2H, $J = 5.50$ Hz). IR (ATR, cm^{-1}): $\nu_{as} = 1337, 1309$; $\nu_{sym} = 1298, 1276$; $\delta_{ONO} = 818, 815$. UV−vis (DMSO, nm (ϵ/(M^{-1} cm^{-1}))): 475 (1.2×10^3), 355 (4.4×10^3), 316 (4.8×10^3), 296 (1.1×10^4).

X-ray Structure Determination. Single crystals were attached to glass fibers and mounted on the Siemens SMART[15] system for data collection at 173(2) K with graphite-monochromated Mo Kα radiation ($\lambda = 0.710\ 73$ Å). An initial set of cell constants was calculated from reflections harvested from three sets of 20 frames oriented such that orthogonal wedges of reciprocal space were surveyed. Orientation matrixes were determined from 35 to 165 reflections. Final cell constants were calculated from a minimum set of 3165 strong reflections from the actual data collection. Data were collected via the hemisphere collection method and surveyed to the extent of 1.3 hemispheres to a resolution of 0.84 Å. Three major swaths of frames with 0.30° steps in ω were collected. The intensity data were corrected for absorption and decay using SADABS.[16] Space groups were determined on the basis of systematic absences and intensity statistics. Direct-methods solutions provided the positions of most non-hydrogen atoms. Several full-matrix least-squares/difference Fourier cycles were performed to locate the remaining non-hydrogen atoms. All calculations were performed using the SHELXTL-V5.0 suite of programs[17] on INDY R4400-SC or Pentium computers. Crystal and X-ray collection and refinement data are summarized in Table 1. Selected bond lengths and angles are given in Table 2.

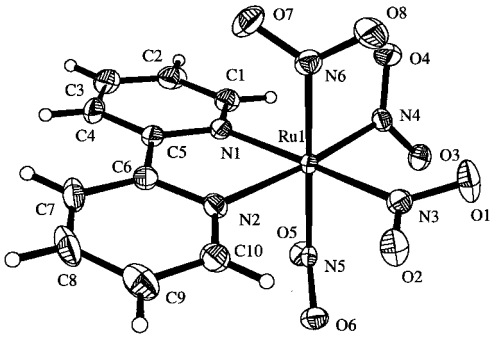

Figure 1. Labeled ORTEP diagram of $[Ru(bpy)(NO_2)_4]^{2-}$ (50% ellipsoids).

$K_2[Ru(bpy)(NO_2)_4]$. Suitable X-ray quality single crystals of $K_2[Ru(bpy)(NO_2)_4]\cdot 4H_2O$ were grown from a water/acetone mixture at −15 °C overnight. An ORTEP diagram of the anion of $K_2[Ru(bpy)(NO_2)_4]$ is shown in Figure 1. Four molecules of water were found in the asymmetric unit. All non-hydrogen atoms were refined with anisotropic displacement parameters. All hydrogen atoms were placed in ideal positions and refined as riding atoms with individual isotropic displacement parameters. Hydrogen atoms on the water molecules were placed in positions reasonable for hydrogen-bonding. One nitro ligand was found to be disordered over two sites, (N3, O1, O2) and (N3′, O1′, O2′). The occupancies of these two sites are 61.35% and 38.65%, respectively. One potassium atom was also found to be disordered over two sites, K2 and K2′. The occupancies of these two sites are 88.42% and 11.58%, respectively.

***fac*-$K[Ru(bpy)(NO_2)_3(py)]$.** A single crystal suitable for an X-ray structural determination was harvested from crystals of *fac*-$K[Ru(bpy)(NO_2)_3(py)]\cdot 2.5H_2O$ grown from a water/acetone mixture. An ORTEP diagram of the anion of *fac*-$K[Ru(bpy)(NO_2)_3(py)]$ is shown in Figure 2. In the asymmetric unit, 2.5 molecules of water were found. All non-hydrogen atoms were refined with anisotropic displacement parameters. All hydrogen atoms were located from the electron density map except the hydrogens bonded to O7 and O8. O7 is disordered over an inversion center. Hydrogens bonded to O7 and O8 form a directed hydrogen-bonding network that points one direction or the opposite direction statistically as caused by the disorder of O7. Hydrogens bonded to O7 and O8 were refined as riding atoms with set isotropic displacement parameters. All remaining hydrogen atoms were refined with individual isotropic displacement parameters.

***cis*-$Ru(NO_2)_2(bpy)(py)_2$.** Single crystals of *cis*-$[Ru(NO_2)_2(bpy)(py)_2]\cdot D_2O$ were grown from a D_2O solution of *fac*-$K[Ru(bpy)(NO_2)_3(py)]$.

(13) The emission spectra were corrected to arbitrary units proportional to photons per energy. For this calculation, see: Blasse, G.; Grabmier, B. C. *Luminescent Materials*, Springer-Verlag: Heidelberg, 1994; p A225.

(14) Ooyama, D.; Miura, Y.; Kanazawa, Y.; Howell, F. S.; Nagao, N.; Mukaida, M.; Nagao, H.; Tanaka, K. *Inorg. Chim. Acta*. **1995**, *237*, 47.

(15) Siemens SMART Platform CCD, Siemens Industrial Automation, Inc., Madison, WI.

(16) An empirical correction for absorption anisotropy: Blessing, R. *Acta Crystallogr*. **1995**, *A51*, 33.

(17) SHELXTL-Plus V5.10, Bruker Analytical X-ray Systems, Madison, WI.

Table 1. Crystal Data, Data Collection, and Refinement Parameters for $K_2[Ru(bpy)(NO_2)_4]\cdot 4H_2O$ (**1**), *fac*-$K[Ru(bpy)(NO_2)_3(py)]\cdot 2.5H_2O$ (**2**), and *cis*-$[Ru(NO_2)_2(bpy)(py)_2]\cdot D_2O$ (**3**)

compd	**1**	**2**	**3**
formula	$C_{10}H_{16}K_2N_6O_{12}Ru$	$C_{15}H_{18}KN_6O_{8.50}Ru$	$C_{20}H_{18}D_2N_6O_5Ru$
habit, color	block, yellow	needle, red	hexagonal plate, red
size, mm	$0.39 \times 0.24 \times 0.21$	$0.25 \times 0.10 \times 0.05$	$0.19 \times 0.19 \times 0.11$
lattice type	monoclinic	monoclinic	monoclinic
space group	$P2_1/c$	$C2/c$	$P2_1/c$
a, Å	11.877(2)	20.277(2)	9.3783(5)
b, Å	12.927(2)	17.703(2)	13.7562(7)
c, Å	13.097(2)	14.823(1)	15.9368(8)
β, deg	99.874(2)	128.973(2)	91.249(1)
V, Å^3	1981.0(4)	4236.4(7)	2055.5(2)
Z	4	8	4
formula wt, g mol^{-1}	591.56	558.52	525.49
D_c, g cm^{-3}	1.983	1.794	1.698
μ, mm^{-1}	1.287	1.019	0.810
$F(000)$	1184	2248	1064
θ range, deg	1.74−25.08	1.73−25.06	1.96−25.03
index ranges	$-12 \le h \le 14$, $-15 \le k \le 14$, $-15 \le l \le 10$	$-18 \le h \le 24$, $-20 \le k \le 21$, $-17 \le l \le 16$	$-11 \le h \le 1$, $-15 \le k \le 16$, $-14 \le l \le 18$
reflns collected	10421	10861	10980
unique reflns	3488 ($R_{int} = 0.0237$)	3649 ($R_{int} = 0.0357$)	3625 ($R_{int} = 0.0281$)
weighting factors,[a] a, b	0.0343, 9.9190	0.0411, 0.0000	0.0377, 0.0000
max, min transmission	1.000000, 0.759817	1.000000, 0.735474	1.000000, 0.893081
data/restraints/parameters	3488/4/313	3649/4/349	3625/0/369
R_1, *wR2* ($I > 2\sigma(I)$)	0.0381, 0.0992	0.0315, 0.0693	0.0283, 0.0610
R_1, *wR2* (all data)	0.0405, 0.1003	0.0568, 0.0778	0.0445, 0.0655
goodness-of-fit (on F^2)	1.166	0.909	0.928
largest diff peak, hole, e Å^{-3}	0.831, −0.615	0.603, −0.454	0.492, −0.367

[a] $w = [\sigma^2(F_o^2) + (aP)^2 + (bP)]^{-1}$, where $P = (F_o^2 + 2F_c^2)/3$.

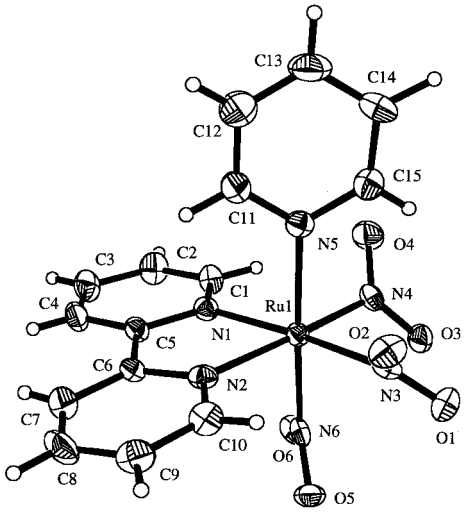

Figure 2. Labeled ORTEP diagram of *fac*-$[Ru(bpy)(NO_2)_3(py)]^-$ (50% ellipsoids).

An ORTEP diagram of *cis*-$[Ru(NO_2)_2(bpy)(py)_2]$ is shown in Figure 3. All non-hydrogen atoms were refined with anisotropic displacement parameters. All hydrogen atoms were located from the electron density map and refined as riding atoms with isotropic displacement parameters. This D_2O molecule forms hydrogen bonds with nitro groups of two different asymmetric units.

Results

Synthesis and Characterization of $[Ru(bpy)(NO_2)_{4-x}(py)_x]^{x-2}$ Complexes. $K_2[Ru(bpy)(NO_2)_4]$ was prepared as shown in Scheme 1. Cleaving the $[(Bz)RuCl_2]_2$ dimer with bpy in refluxing acetonitrile solution produces [(Bz)Ru(bpy)Cl]Cl. Refluxing [(Bz)Ru(bpy)Cl]Cl with an excess of KNO_2 produces $K_2[Ru(bpy)(NO_2)_4]$ in good yield as a bright yellow-orange powder. The product is easily purified by recrystallization from water/methanol to give material with an acceptable elemental analysis. $K_2[Ru(bpy)(NO_2)_4]$ is indefinitely stable as a solid. In aqueous solution, it decomposes over several hours to give a variety of unidentified products.

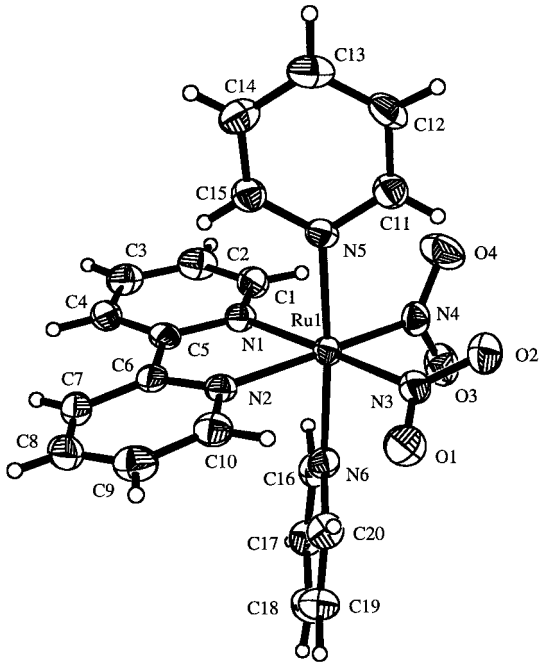

Figure 3. Labeled ORTEP diagram of *cis*-$[Ru(NO_2)_2(bpy)(py)_2]$ (50% ellipsoids).

In contrast to the inert behavior of most ruthenium(II) benzene complexes with respect to thermally induced replacement reactions,[1−4,18−21] the reaction between [(Bz)Ru(bpy)Cl]Cl and KNO_2 occurs at room temperature with displacement of the benzene ligand as was monitored by ^{1}H NMR spectroscopy.

(18) Bennett, M. A.; Smith, A. K. *J. Chem. Soc., Dalton Trans*. **1974**, 233.

Table 2. Selected Bond Lengths (Å) and Angles (Deg)[a] for $K_2[Ru(bpy)(NO_2)_4]\cdot 4H_2O$ (**1**), *fac*-$K[Ru(bpy)(NO_2)_3(py)]\cdot 2.5H_2O$ (**2**), and *cis*-$[Ru(NO_2)_2(bpy)(py)_2]\cdot D_2O$ (**3**)

	compd		
	1	**2**	**3**
Ru(1)−N(1)	2.083(4)	2.087(4)	2.077(2)
Ru(1)−N(2)	2.103(4)	2.116(4)	2.084(2)
Ru(1)−N(3)	2.028(10), 2.06(2)[b]	2.038(4)	2.049(2)
Ru(1)−N(4)	2.024()	2.024(4)	2.033(2)
Ru(1)−N(5)	2.044(4)	2.125(4)	2.124(3)
Ru(1)−N(6)	2.045(4)	2.024(4)	2.099(2)
N(3)−O(1)	1.257(5), 1.258(5)[b]	1.255(5)	1.249(3)
N(3)−O(2)	1.257(5), 1.258(5)[b]	1.253(5)	1.245(3)
N(4)−O(3)	1.263(5)	1.272(5)	1.248(3)
N(4)−O(4)	1.255(5)	1.254(5)	1.246(3)
N(5)−O(5)	1.250(5)	*c*	*c*
N(5)−O(6)	1.256(5)	*c*	*c*
N(6)−O(5)	*c*	1.261(5)	*c*
N(6)−O(6)	*c*	1.250(5)	*c*
N(6)−O(7)	1.254(5)	*c*	*c*
N(6)−O(8)	1.266(5)	*c*	*c*
N(1)−Ru(1)−N(2)	78.1(2)	77.64(15)	78.27(9)
N(1)−Ru(1)−N(3)	176.6(2)	174.15(15)	177.28(10)
N(1)−Ru(1)−N(4)	94.8(2)	95.01(15)	94.94(9)
N(1)−Ru(1)−N(5)	90.42(14)	93.46(14)	89.63(9)
N(1)−Ru(1)−N(6)	89.7(2)	87.60(15)	88.97(9)
N(2)−Ru(1)−N(3)	98.7(2)	96.54(16)	99.10(9)
N(2)−Ru(1)−N(4)	172.8(2)	172.15(15)	172.29(9)
N(2)−Ru(1)−N(5)	89.46(14)	93.62(14)	90.64(9)
N(2)−Ru(1)−N(6)	90.0(2)	89.21(15)	85.09(9)
N(3)−Ru(1)−N(4)	88.4(2)	90.76(15)	87.72(9)
N(3)−Ru(1)−N(5)	90.6(4)	87.52(15)	89.68(9)
N(3)−Ru(1)−N(6)	89.3(4)	91.69(16)	91.53(9)
N(4)−Ru(1)−N(5)	91.6(2)	89.55(15)	92.99(10)
N(4)−Ru(1)−N(6)	89.0(2)	87.70(15)	91.23(10)
N(5)−Ru(1)−N(6)	179.4(2)	177.13(15)	175.65(9)
O(1)−N(3)−O(2)	112.9(9), 120(2)[b]	116.8(4)	115.2(2)
O(3)−N(4)−O(4)	116.4(4)	116.8(4)	116.0(3)
O(5)−N(5)−O(6)	117.3(4)	*c*	*c*
O(5)−N(5)−O(6)	c	116.8(4)	*c*
O(7)−N(6)−O(8)	115.8(4)	*c*	*c*

[a] Estimated standard deviation in the least significant figure are given in parentheses. [b] Minor component of a disordered nitro group. [c] Not applicable.

Scheme 1

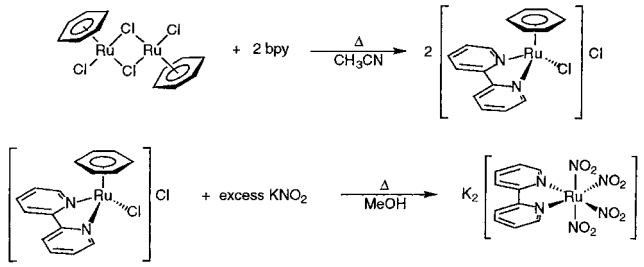

The initial spectrum shows a singlet for the η^6-benzene ring bound to the ruthenium at 6.15 ppm. Within 5 min after the addition of KNO_2, two new peaks appear, a singlet at 7.32 ppm that is assigned to free benzene and a small peak at 6.26 ppm. No peaks are observed for the product ($[Ru(bpy)(NO_2)_4]^{2-}$ anion) because of its extremely low solubility in methanol (a precipitate began to form in the NMR tube after several hours).

Reaction of $K_2[Ru(bpy)(NO_2)_4]$ with pyridine results in the substitution of one or two nitro ligands, depending on the reaction conditions. At room temperature, $K_2[Ru(bpy)(NO_2)_4]$ reacts with an excess of pyridine in aqueous solution to yield the monosubstituted pyridine complex *fac*-$K[Ru(bpy)(NO_2)_3(py)]$ as a reddish-orange solid. The stoichiometry of this complex was confirmed by elemental analysis. If $K_2[Ru(bpy)(NO_2)_4]$ is refluxed in pyridine containing a small amount of water, a dark red precipitate forms over several days. The isolated red solid has an elemental analysis and spectroscopic parameters consistent with the neutral disubstituted pyridine complex *cis*-$[Ru(NO_2)_2(bpy)(py)_2]$ complex. This complex was prepared previously by a different route, but only limited spectroscopic data were reported.[14]

NMR Studies. The protons on the 2,2′-bipyridine rings provide an excellent probe for the geometry around the ruthenium. The ^{1}H NMR of $K_2[Ru(bpy)(NO_2)_4]$ was acquired in D_2O solution. Four resonances for the eight bipyridine protons were observed, consistent with the expected C_{2v} symmetry of this complex. If the NMR spectrum was acquired within 10 min of dissolution, only these peaks were observed. After 10 min, several new sets of bipyridine resonances were also observed, indicating reactions of the complex with water occur. The products of the reaction suggest that the formal loss of O^{2-} from a nitro group yields complexes with nitrosyl ligands. Studies are in progress to characterize this reaction and will be reported in the future.

The ^{1}H NMR of *fac*-$K[Ru(bpy)(NO_2)_3(py)]$, also in D_2O solution, shows four resonances assigned to the bipyridine ligand and three resonances assigned to the pyridine ligand. This pattern is consistent with the *fac* isomer (C_s symmetry) (confirmed by X-ray crystallography). The ^{1}H NMR of *cis*-$[Ru(NO_2)_2(bpy)(py)_2]$ in DMSO-d_6 solution also shows four resonances that are assigned to the bipyridine ligand and three resonances that are assigned to the pyridine ligands. These data are consistent with either nitro or pyridine ligands occupying both positions trans to the bipyridine ligand; the *fac* geometry of the $[Ru(bpy)(NO_2)_3(py)]^-$ ion suggests that the second pyridine occupies the position trans to the first pyridine ligand. This geometry was also confirmed by X-ray crystallography.

Infrared Spectroscopy. The infrared spectra of the three nitro complexes are complicated. Metal−nitro complexes typically exhibit three infrared bands, symmetric (ν_s) and asymmetric stretching modes (ν_{as}) and bending (δ).[22] Taking into account the low symmetry in the solids, all possible nitro-centered vibrational modes are expected to be active. $K_2[Ru(bpy)(NO_2)_4]$ exhibits two groups of peaks centered around 1340 and 1280 cm^{-1}, typical positions for the asymmetric and symmetric stretching modes, respectively. Each group represents three or four different peaks that are very close in energy. In addition, four sharp, well-defined peaks are observed at 833, 824, 821, and 802 cm^{-1}, typical energies for the scissoring mode. The *fac*-$K[Ru(bpy)(NO_2)_3(py)]$ complex displays peaks at 1320 and 1303 cm^{-1} assigned to asymmetric stretches and 1275 and 1212 cm^{-1} assigned to the symmetrical stretching modes. There is also a peak at 822 cm^{-1} with a low energy shoulder that is assigned to the scissoring mode. The IR spectrum of *cis*-$[Ru(NO_2)_2(bpy)(py)_2]$ displays peaks at 1337 and 1309 cm^{-1} assigned to asymmetric NO_2 stretches and 1298 and 1276 cm^{-1} assigned to the symmetric NO_2 stretches. The two peaks at 818 and 815 cm^{-1} are assigned to ONO scissoring modes.

X-ray Studies. Single-crystal X-ray data were obtained for all three compounds and are reported here. For all three

(19) Bennett, M. A.; Matheson, T. W.; Robertson, G. B.; Smith, A. K.; Tucker, P. A. *Inorg. Chem.* **1980**, *19*, 1014.
(20) Weber, W.; Ford, P. C. *Inorg. Chem.* **1986**, *25*, 1088.
(21) Karlen, T.; Hauser, A.; Ludi, A. *Inorg. Chem.* **1986**, *25*, 1088.
(22) Cotton, F. A.; Wilkinson, G. *Advanced Inorganic Chemistry*, 5th ed.; Wiley: New York, 1988; p 486.

compounds, the nitro groups in the same plane as the bipyridine rings will be referred to as trans while the mutually trans ligands cis to both rings of the bipyridine ligand will be referred to as cis.

The structure of $[Ru(bpy)(NO_2)_4]^{2-}$ shows (Figure 1) that the nitro groups are all coordinated via nitrogen. The packing diagram of $[Ru(bpy)(NO_2)_4]^{2-}$ (Figure S1, Supporting Information) shows that channels are created by columns of the $[Ru(bpy)(NO_2)_4]^{2-}$ anions (water molecules and potassium cations that fill these channels are omitted for clarity). Water molecules are located within hydrogen-bonding distances of the nitro ligands. The anion columns are oriented so the hydrophilic nitro groups line the channels. The bpy ligands, which point away from the channels, form similar hydrophobic layers. One of the trans nitro ligands was found to be disordered over two sites. The *trans*-nitro ligands are canted with respect to the bipyridine ring. The angles between the least squares plane containing the bpy ring and the least-squares planes containing the trans nitro groups and the ruthenium are 19.4° (O(1),N(3),O(2)), 31.9° (O(1′),N(3′),O(2′)), and 59.7° (O(4),N(4),O(3)). The bond lengths between the ruthenium and the trans nitro ligands are essentially identical at 2.028 and 2.024 Å. The cis nitro ligands are oriented so that the least-squares planes containing the nitro groups and the ruthenium are not far from being perpendicular to one another (69.2°). The bond lengths between the ruthenium and the nitrogens of these nitro groups are nearly equal (2.044 and 2.045 Å) but significantly longer then the trans Ru−NO_2 bond lengths. The geometry around the ruthenium is essentially octahedral with some distortion due to the bite angle of the bpy ligand (N(1)−Ru-N(2) angle of 78.1°). The angles between the bpy nitrogens and the nitrogens on the cis nitro groups are correspondingly greater than 90° (98.7° and 94.8°). The bpy ligand is not completely symmetrical with two Ru− N(bpy) bonds of 2.103 and 2.083 Å.

The ORTEP diagram of *fac*-$[Ru(bpy)(NO_2)_3(py)]^-$ (Figure 2) confirms that the nitro groups are all bound via nitrogen and that the complex forms as the *fac* isomer as suggested by the ^{1}H NMR data. The packing diagram (Figure S2, Supporting Information) is similar to that of $[Ru(bpy)(NO_2)_4]^{2-}$ with columns of anions and hydrophobic layers of bpy groups. The nitro groups again line channels filled with potassium cations and water molecules. A hydrogen-bonding network of water molecules is present in the hydrophilic channels. The least-squares planes of the nitro ligands trans to bpy are canted at similar angles (52.6 and 57.0°) but in the opposite direction with respect to the plane of the bipyridine ring. The Ru−NO_2 (trans) bond lengths differ slightly (2.040 and 2.023 Å). The nitro group cis to bpy has a similar Ru−NO_2 bond length of 2.025 Å. The plane containing this nitro group is oriented so that it is approximately perpendicular to the plane of symmetry, which bisects the bipyridine ligand. The pyridine ligand trans to this nitro is almost perpendicular with an 87.5° angle between the least-squares planes containing the pyridine and the nitro group. This places the pyridine almost parallel with the plane of symmetry bisecting the bipyridine ligand. The pyridine ligand is tipped toward the nitro ligands trans to the bipyridine with angles of 89.51 and 86.55° between the pyridine nitrogen and the trans nitro nitrogens and angles of 93.46 and 93.62° between the pyridine nitrogen and the two bipyridine nitrogens. The Ru−N(pyridine) bond distance is 2.125 Å, substantially longer than both the Ru−N(bpy) and Ru−NO_2 bond distances.

The ORTEP representation of *cis*-$[Ru(NO_2)_2(bpy)(py)_2]$ (Figure 3) shows that all of the nitro groups are N-bound and that the complex forms with the pyridine groups trans and the nitro groups cis. In contrast to the structure determined for $K_2[Ru(bpy)(NO_2)_4]\cdot 4H_2O$ and *fac*-$K[Ru(bpy)(NO_2)_3(py)]\cdot 2.5H_2O$, obvious solvent channels are not present in the packing diagram (Figure S3, Supporting Information). The D_2O molecule located in the lattice is however within hydrogen-bonding distances of two different *cis*-$[Ru(NO_2)_2(bpy)(py)_2]$ units. The two nitro groups are canted with respect to the bpy ring by angles of 20.0 and 89.7°. The Ru−NO_2 bond lengths are 2.033 and 2.049 Å. One pyridine ligand is essentially perpendicular to the plane of symmetry bisecting the bipyridine ligand. This pyridine bends slightly toward the bipyridine ligand with angles of 85.09 and 88.97° between the pyridine nitrogen and the bipyridine nitrogens and angles of 91.53 and 91.23° to the nitro groups. The second pyridine ligand is not far from being perpendicular to the first, with an angle of 77.7° between the pyridine least-squares planes. The other pyridine ligand "leans" toward the bipyridine ring with N(6)−Ru−N(1) and N(6)−Ru−N(2) bond angles of 88.97 and 85.09°, respectively. The angles to the nitro ligands (N(6)−Ru−N(3) and N(6)−Ru−N(4)) are correspondingly greater than 90° (91.53 and 92.99°). The Ru−N(pyridine) bond lengths are significantly different (2.099 and 2.124 Å), with the shorter bond to the pyridine that is perpendicular to the plane of symmetry bisecting the bpy ligand. It is interesting to note that the length of the longer of the two Ru−N(pyridine) bonds in *cis*-$[Ru(NO_2)_2(bpy)(py)_2]$ is essentially identical to the Ru−N(pyridine) bond length in $[Ru(bpy)(NO_2)_3(py)]^-$ and that both of these pyridine ligands have the same orientation relative to the bpy ligand.

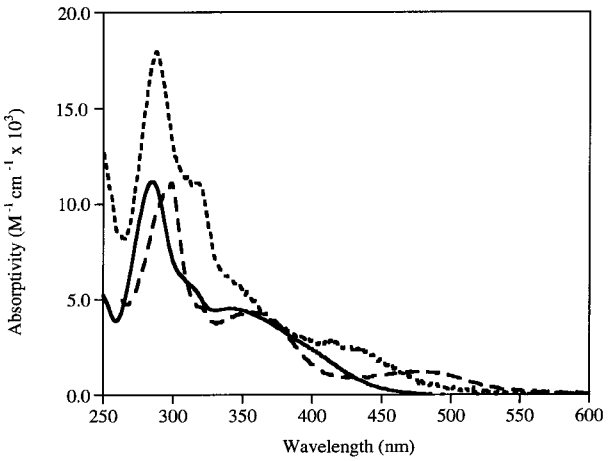

Figure 4. UV−vis absorption spectra of $K_2[Ru(bpy)(NO_2)_4]$ (aqueous solution, —), *fac*-$K[Ru(bpy)(NO_2)_3(py)]$ (aqueous solution, - - -), and *cis*-$[Ru(NO_2)_2(bpy)(py)_2]$ (DMSO solution, — — —).

Absorption and Emission Studies. Absorption spectra of $K_2[Ru(bpy)(NO_2)_4]$ and *fac*-$K[Ru(bpy)(NO_2)_3(py)]$ in water and *cis*-$[Ru(NO_2)_2(bpy)(py)_2]$ in DMSO have been collected and are shown in Figure 4. Absorption maxima and extinction coefficients are given in the Experimental Section. No extinction coefficients are given for $K_2[Ru(bpy)(NO_2)_4]$ due to its instability in aqueous solution. The region from 285 to 319 nm is very similar for all three compounds. The intense band in each complex at 285−296 nm is assigned to bpy $\pi \rightarrow \pi^*$ transitions by comparison with other Ru(II)bpy complexes.[23] The shoulder in each complex in the region of 313−319 nm is not observed in the related cyano complexes such as $[Ru(bpy)(CN)_4]^{2-}$, suggesting that they involve the nitro groups. It is possible that

(23) Balzani, V.; Boletta, E.; Gandolfi, M. T.; Maestri, M. *Top. Curr. Chem.* **1978**, *75*, 1.

Table 3. Position of the Lowest Energy MLCT Absorption Maximum as a Function of Solvent for $K_2[Ru(bpy)(NO_2)_4]$ and *fac*-$K[Ru(bpy)(NO_2)_3(py)]$

		λ_{max} (nm)	
solvent	AN[a]	$K_2[Ru(bpy)(NO_2)_4]$	*fac*-$K[Ru(bpy)(NO_2)_3(py)]$
H_2O	54.8	390	402
CH_3OH	41.3	423	438
1-propanol	33.5	437	452
CH_2Cl_2	20.4	478	*b*
CH_3CN	19.3	479	*b*
DMSO	19.3	493	*b*
DMF	16.0	506	*b*
acetone	12.5	512	510

[a] Gutmann acceptor number. [b] Data not collected.

they are either nitro-localized n → π^* or $\pi \rightarrow \pi^*$ transitions or a dπ(Ru) → $\pi^*(NO_2)$ MLCT transition. Assignment as an intraligand transition is consistent with the observation that this absorption band is not solvatochromic. The shoulders in the spectra of $K_2[Ru(bpy)(NO_2)_4]$ and *fac*-$K[Ru(bpy)(NO_2)_3(py)]$ and the absorption band of *cis*-$[Ru(NO_2)_2(bpy)(py)_2]$ in the region of 340−355 nm are assigned to a high energy component of the dπ(Ru) → π^*(bpy) MLCT transition. This higher energy MLCT component is more evident in spectra of the compounds in solvents of low acceptor number (vide infra) where the band is shifted to longer wavelength. The absorption bands in the region from 390 to 475 nm are assigned as low energy MLCT dπ(Ru) → π^*(bpy) transitions. The assignment of these two bands as dπ(Ru) → π^*(bpy) MLCT transitions is consistent with the large solvatochromic shifts observed and the absorption spectrum of $[Ru(bpy)(CN)_4]^{2-}$.[6]

We investigated the solvent dependence of the absorption spectrum of $K_2[Ru(bpy)(NO_2)_4]$ and *fac*-$K[Ru(bpy)(NO_2)_3(py)]$. Although both complexes have minimal solubility in solvents other than water, the addition of [2.2.2]crypt greatly enhanced the solubility of the potassium salts in organic solvents and allowed absorption spectra to be determined in a variety of solvents (Table 3). The lowest energy MLCT absorption bands of $K_2[Ru(bpy)(NO_2)_4]$ and $K[Ru(bpy)(NO_2)_3(py)]$ exhibit significant solvatochromism. Plots of the energy of the maxima of the longest wavelength absorption bands vs the acceptor number (AN) of the solvent are shown in Figure 5. Good, linear correlations are observed for both compounds. The slopes and intercepts of the best fit lines are given in Figure 5.

Emission spectra of solids and solutions of $K_2[Ru(bpy)(NO_2)_4]$, *fac*-$K[Ru(bpy)(NO_2)_3(py)]$, and *cis*-$[Ru(NO_2)_2(bpy)(py)_2]$ have been collected at room temperature. The emission maxima of the three solids are 610, 650, and 685 nm, respectively, as shown in Figure 6. Vibronic structure in the complex *cis*-$[Ru(bpy)(NO_2)_2(py)_2]$ is consistent with significant distortion of the bpy ligand in the MLCT excited states, as is also found for the complex *cis*-$Ru(bpy)_2(NO_2)_2$.[24] The assignment of these emission bands as arising from dπ(Ru) → π^*-(bpy) MLCT excited states is consistent with the vibronic structure, the shift of the band energies to lower energy with increased pyridine substitution, and comparison with similar Ru^{II} bpy complexes.[24,25] No emission was detected from deaerated water solutions of $K_2[Ru(bpy)(NO_2)_4]$ and *fac*-$K[Ru(bpy)(NO_2)_3(py)]$; however, emission from a deaerated DMSO solution of *cis*-$[Ru(NO_2)_2(bpy)(py)_2]$ was observed with an emission maximum of 699 nm.

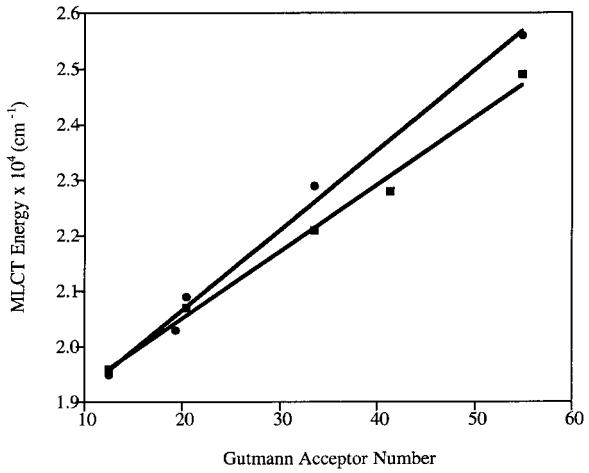

Figure 5. Shifts in (a) E_{abs}(MLCT) for $K_2[Ru(bpy)(NO_2)_4]$ and (b) *fac*-$K[Ru(bpy)(NO_2)_3(py)]$ vs solvent acceptor number. Lines are best fit lines based on linear regression analysis. Fitting parameters: (a) slope = 144 ± 7 cm^{-1}/AN, intercept = 17700 ± 200 cm^{-1}, R^2 = 0.987; (b) slope = 121 ± 6 cm^{-1}/AN intercept = 18100 ± 200 cm^{-1}, R^2 = 0.991.

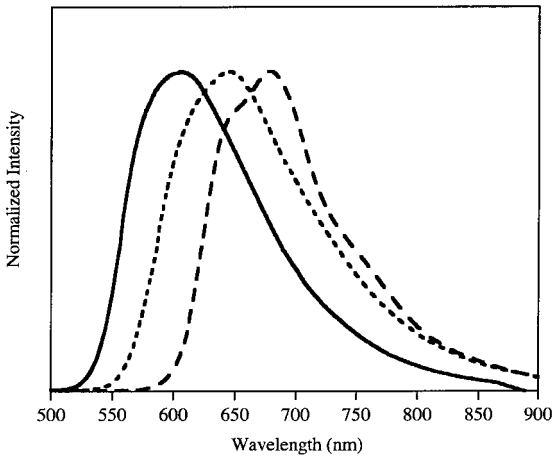

Figure 6. Normalized solid-state emission spectra of $K_2[Ru(bpy)(NO_2)_4]$ (—), *fac*-$K[Ru(bpy)(NO_2)_3(py)]$ (- - -), and *cis*-$[Ru(NO_2)_2(bpy)(py)_2]$ (— — —).

Discussion

The facile formation of the $[Ru(bpy)(NO_2)_4]^{2-}$ ion via the thermal displacement of benzene from [(Bz)Ru(bpy)Cl]Cl is surprising. Although there are numerous examples[1−4,18,20,21] of the photochemical displacement of benzene from Ru(II), there are only a few examples, to our knowledge, of thermal displacement.[18,19,26,27] To gain some additional mechanistic insight, the reaction of $[(Bz)Ru(bpy)Cl]^+$ with a large excess of nitrite ion was monitored by ^1H NMR spectroscopy. The bound and free benzene resonances provide an excellent probe for the extent of the reaction. The decrease in intensity of the bound benzene peak is concomitant with the increase in intensity of the free benzene peak. The small singlet at 6.26 ppm is presumably a coordinated benzene resonance of an intermediate in the formation of $[Ru(bpy)(NO_2)_4]^{2-}$ from $[(Bz)Ru(bpy)Cl]^+$ that is present almost immediately after the reaction is initiated and remains until almost all of the starting material is consumed.

(24) Bignozzi, C. A.; Chiorboli, C.; Murtaza, A.; Jones, W. E.; Meyer, T. J. *Inorg. Chem.* **1993**, *32*, 1036.
(25) Krause, R. A.; Ballhausen, C. J. *Acta Chem. Scand. A.* **1977**, *31*, 535.
(26) Green, M. L. H.; Joyner, D. S.; Wallis, J. M. *J. Chem. Soc., Dalton Trans.* **1987**, 2823.
(27) Tobita, H.; Hasegawa, K.; Minglana, J. J. G.; Luh, L.-S.; Okazaki, M.; Ogino, H. *Organometallics.* **1999**, *18*, 2058.

It is reasonable to assign this peak to the benzene resonance of $[(Bz)Ru(bpy)(NO_2)]^+$, formed by the reaction of $[(Bz)Ru(bpy)Cl]^+$ with nitrite ion. The small shift for this peak relative to the benzene peak for $[(Bz)Ru(bpy)Cl]^+$ is consistent with replacement of chloride with nitro. Preliminary kinetic data indicate the reaction is first order with respect to the ruthenium complex. Previous kinetic studies of arene displacement from Ru(II) arene complexes[28,29] suggest that arene displacements proceed through reduced hapticity intermediates (η^2 or η^4). Perhaps the nitro group stabilizes the transition state in a slipped ring intermediate by occupying the additional empty coordination site. It is interesting to note that attempts to prepare $[(Bz)Ru(bpy)(NO_2)]^+$ by reacting $[(Bz)Ru(bpy)Cl]^+$ with only 1 equiv of nitrite ion, produced $[Ru(bpy)(NO_2)_4]^{2-}$ along with starting material. Further mechanistic studies are in progress.

The bond lengths and angles determined crystallographically for all three compounds are reasonable for ruthenium-nitro complexes. The $Ru-NO_2$ bond lengths range mainly from 2.024(4) to 2.049(2) Å with the exception of the minor component of the disordered nitro group in $[Ru(bpy)(NO_2)_4]^{2-}$ (Ru(1)−N(3′), 2.06(2) Å). Comparison with other Ru(II) complexes indicates that these values are slightly shorter than ones typically observed.[30−33] For instance, the $Ru-NO_2$ bond distances are 2.074 Å for *trans*-$[Ru(tpy)(PMe_3)_2(NO_2)](ClO_4)$[30] (tpy = 2,2′:6′,2″-terpyridine), 2.078 and 2.080 Å for $Na_2[Ru(NO_2)_4(NO)(OH)]$,[31] 2.20 Å for *cis*-$[Ru(bpy)_2(CO)(NO_2)](PF_6)$,[32] and 2.060 Å for $Na_2[Ru(NO_2)_6]$.[33] For the first three complexes, the longer $Ru-NO_2$ bond distance can be attributed either to the overall positive charge of the complex or the presence of other strong π-accepting ligands such nitrosyl or carbonyl. Both factors would decrease the amount of back-bonding from the ruthenium to the nitro group(s).

There is a notable similarity in the relative orientation of the two ligands cis to bipyridine. In all three structures, these ligands, either pyridine or nitro, are oriented with one ligand nearly parallel to the plane of symmetry bisecting the bipyridine ligand and the other ligand is oriented nearly perpendicular to the first. The relative orientation of these two ligands can be attributed to the ability of nitro and pyridine to back-bond only in the plane perpendicular to the plane of the ligand. The nearly orthogonal orientation of the cis ligands allows them to withdraw electron density from separate d orbitals. This same argument also applies to the bipyridine ligand and the trans nitro groups, but in this case, bipyridine is not free to rotate and the nitro ligands trans to bpy exhibit no consistent orientation relative to the plane of the bipyridine ligand. The angles between the least squares planes containing the bipyridine ligand and the least squares plane containing the trans nitro ligands and the ruthenium range from 17° to almost 90°. The orientations observed may be the result of other factors, such as crystal packing forces. However, some variation in the $Ru-NO_2$ and Ru−N(bpy) bond lengths as a function of the bipyridine and trans nitro group least-squares planes angle would be anticipated. The Ru−N(bpy) bond lengths in $[Ru(bpy)(NO_2)_4]^{2-}$ and $[Ru(bpy)(NO_2)_3(py)]^-$ differ by 0.020 and 0.029 Å, respectively, while the two Ru−N(bpy) bonds in *cis*-$[Ru(NO_2)_2(bpy)(py)_2]$ differ by only 0.007 Å.

The absorption and emission spectra of the nitro complexes described here display some interesting similarities to and differences from the analogous cyanide complexes. The absorption spectra are very similar to those of the cyanide complexes, displaying bands that can by assigned by analogy to $d\pi(Ru) \rightarrow \pi^*(bpy)$ charge transfer and $\pi(bpy) \rightarrow \pi^*(bpy)$ transitions. As with the cyanide complexes, substitution of anionic ligands with pyridine shifts both MLCT bands to lower energies. This is attributed to the weaker π-accepting ability of pyridine relative to nitro. Qualitatively, the emission behavior of the nitro complexes differs from the cyano complexes in that the $RuL_x(CN)_{6-x}$ ($x = 0-5$; L is a pyridine-type ligand) complexes are all emissive at room temperature in fluid solution while $K_2[Ru(bpy)(NO_2)_4]$ and *fac*-$K[Ru(bpy)(NO_2)_3(py)]$ display emission as solids, but not in aqueous solution. This result is consistent with deactivation of the emissive MLCT state by a putative d−d state. For mixed ligand Ru(bpy) complexes, Hoggard et al.[10] determined the angular overlap parameters for nitro to be $e_\pi = -1160\ cm^{-1}$; $e_\sigma = 6700\ cm^{-1}$ and cyanide to be $e_\pi = -620\ cm^{-1}$; $e_\sigma = 10{,}800\ cm^{-1}$, giving $\Delta_{nitro} = 24\,700\ cm^{-1}$ and $\Delta_{cyanide} = 34\,800\ cm^{-1}$. The weaker ligand field generated by the nitro ligands probably positions a d−d state at an energy low enough to quench the emission from the MLCT excited states in aqueous solution; however, we do observe room-temperature emission from *cis*-$[Ru(NO_2)_2(bpy)(py)_2]$ in DMSO solution.

The solvatochromism of the lowest energy MLCT bands of $K_2[Ru(bpy)(NO_2)_4]$ and *fac*-$K[Ru(bpy)(NO_2)_3(py)]$ correlate linearly with the Gutmann acceptor number (Figure 5) and the number of nitro ligands present. The slopes of the MLCT energy vs AN plots ($\Delta E/\Delta AN$) are a measurement of the sensitivity of the complex to solvent influences. The value of $\Delta E/\Delta AN$ for $[Ru(bpy)(NO_2)_4]^{2-}$ ($146 \pm 7\ cm^{-1}$/AN) is larger than that of $[Ru(bpy)(NO_2)_3(py)]^-$ ($120 \pm 6\ cm^{-1}$/AN). The similarity in the values of $\Delta E/\Delta AN$ per nitro ligand for $[Ru(bpy)(NO_2)_4]^{2-}$ (36.5 cm^{-1}/AN/NO_2^-) and for $[Ru(bpy)(NO_2)_3(py)]^-$ (40 cm^{-1}/AN/NO_2^-) suggests that the contribution of each nitro ligand is nearly additive with respect to the solvatochromic sensitivity of the complex. These findings are in qualitative agreement with those reported in a study by Timpson et al.,[6] who demonstrated a strong linear correlation of the energy of the lowest MLCT absorption band and the Gutmann solvent acceptor number for the analogous cyano complexes $RuL_x(CN)_{6-x}$. This study also indicated that the shifts in MLCT absorption bands increase linearly with the number of cyano ligands. For the cyano complexes, plots of the lowest MLCT band energies vs a function based on the solvent dielectric constant show only a weak correlation. Timpson et al.[6] suggest that the solvatochromism of $RuL_x(CN)_{6-x}$ complexes is due to *specific* donor−acceptor interactions between the solvent and the lone pair on the nitrogen of the cyanide ligands. Qualitatively, our data for the nitro complexes suggest that the solvatochromic shift mechanisms for the nitro and cyano complexes are similar; however, quantitative considerations lead to a more complicated conclusion. For example, the values of $\Delta E/\Delta AN$ for the energy/Gutmann AN correlations for $[Ru(bpy)(NO_2)_4]^{2-}$ and $[Ru(bpy)(CN)_4]^{2-}$ ($146 \pm 7\ cm^{-1}$/AN vs $140 \pm 17\ cm^{-1}$/AN) are identical within experimental error. Additionally, the contributions per ligand to the solvatochromic shifts (calculated over a series of complexes, each for nitro and cyano complexes[6]) ($37 \pm 4\ cm^{-1}$/AN/NO_2^- and $35 \pm 3\ cm^{-1}$/AN/CN^-) are also

(28) Koefod, R. S.; Mann, K. R. *J. Am. Chem. Soc.* **1990**, *112*, 7287.
(29) McNair, A. M.; Mann, K. R. *Inorg. Chem.* **1986**, *25*, 2519.
(30) Leising, R. A.; Kubow, S. A.; Churchill, M. R.; Buttrey, L. A.; Ziller, J. W.; Takeuchi, K. J. *Inorg. Chem.* **1990**, *29*, 1306.
(31) Blake, A. J.; Gould, R. O.; Johnson, B. F. G.; Parisini, E. *Acta Crystallogr.* **1992**, *C48*, 982.
(32) Tanaka, H. Nagao, H.; Tanaka, K. *Inorg. Chem.* **1992**, *31*, 1971.
(33) Gromilov, S. A.; Alekseev, V. I.; Vyacheslav, A. E.; Baidina, I. A. *Acta Crystallogr.* **1996**, *C52*, 288.

essentially the same. If the solvatochromic shift mechanism actually involves specific cyano or nitro/solvent interactions, the significant difference in σ-donor and π-acceptor abilities between the nitro and cyano ligands might be expected to give quantitative differences in the $\Delta E/\Delta AN$ and $\Delta E/\Delta AN$/ligand values. Instead, the $\Delta E/\Delta AN$ and $\Delta E/\Delta AN$/ligand values are nearly identical. Why?

If a specific solvent−ligand interaction mechanism is invoked to describe the behavior of the nitro complexes, the nitro and cyano ligands are required to have identical relative interactions with a wide range of solvents, which is unreasonable. The similarity in the behavior of the complexes could be coincidental, but this is also unlikely. A third explanation of this result is that nonspecific interactions of solvent with the chromophore are the cause of the MLCT band shifts. This explanation also presents some difficulties. If the solvatochromism was due to nonspecific interactions then one might expect the absorption band energies to correlate with a function of the solvent dielectric constant (as is observed with $[Ru(bpy)_3]^{2+}$ [34]) rather than the acceptor number. More work will be needed to explain the combined nitro and cyano complex behavior. The successful explanation of this phenomenon must take into account the following: (1) the absorption band energy dependence on solvent acceptor number; (2) the dependence on the number of nitro or cyano ligands; and (3) the differences in the properties of the nitro and cyano ligands. We intend to pursue this by investigating the spectroscopic properties of analogous ruthenium complexes containing small anionic ligands other than cyanide and nitrite.

(34) Kober, E. M.; Sullivan, B. P.; Meyer, T. J. *Inorg. Chem.* **1984**, *23*, 2098.

Conclusions

We have demonstrated that thermal arene displacement from $[(Bz)Ru(bpy)Cl]^+$ is an effective route to the new $K_2[Ru(bpy)(NO_2)_4]$ complex. Our data suggest that the displacement of benzene under such mild conditions is caused by introducing a nitro ligand into the coordination sphere of the ruthenium. We are currently engaged in mechanistic studies to further elucidate the details of this reaction. The tetranitro complex is a useful starting material for the preparation of *fac*-$K[Ru(bpy)(NO_2)_3(py)]$ and *cis*-$[Ru(NO_2)_2(bpy)(py)_2]$. Crystal structures were obtained for all three complexes. As with the analogous cyanide complexes, the nitro complexes display significant solvatochromism of the low energy, intense MLCT bands. Despite the significant differences between the π-accepting ability of the nitro and cyano ligands, the solvatochromic behavior of the two sets of complexes are quantitatively identical. Further studies will be required to successfully describe the nuances of the solvatochromism in these complexes.

Acknowledgment. D.A.F. wishes to acknowledge the financial support of The State University of New York at New Paltz. K.R.M. acknowledges the financial support of the National Science Foundation under Grant No. CHE-9307837.

Supporting Information Available: X-ray crystallographic files in CIF format for $K_2[Ru(bpy)(NO_2)_4]\cdot 4H_2O$, *fac*-$K[Ru(bpy)(NO_2)_3(py)]\cdot 2.5H_2O$, and *cis*-$[Ru(NO_2)_2(bpy)(py)_2]\cdot D_2O$ and solid-state packing diagrams of *fac*-$K[Ru(bpy)(NO_2)_3(py)]\cdot 2.5H_2O$ and *cis*-$[Ru(NO_2)_2(bpy)(py)_2]\cdot D_2O$. This material is available free of charge via the Internet at http://pubs.acs.org.

IC010548M